International Symposium
On Turbulence and Shear Flow
Phenomena (TSFP-8)
August 28 - 30, 2013 Poitiers, France

DYNAMICS OF ELASTO-INERTIAL TURBULENCE IN FLOWS WITH POLYMER ADDITIVES

Vincent E. Terrapon
Aerospace and Mechanical Engineering Department
University of Liege
1 Ch. des Chevreuils
4000 Liege, Belgium
vincent.terrapon@ulg.ac.be

Yves Dubief
School of Engineering
University of Vermont
201 Votey Bldg
Burlington, Vermont, VT 05405, USA
ydubief@uvm.edu

Julio Soria
Aerospace and Mechanical Engineering Department
Monash University
Building 33, Clayton Campus
Monash University,VIC 3800, Australia
julio.soria@monash.edu
Department of Aeronautical Engineering
King Abdulaziz University, Jeddah, Kingdom of Saudi Arabia

ABSTRACT

The dynamics of elasto-inertial turbulence is investigated numerically from the perspective of the coupling between polymer dynamics and flow structures. In particular, direct numerical simulations of channel flow with Reynolds numbers ranging from 1000 to 6000 are used to study the formation and dynamics of elastic instabilities and their effects on the flow. Based on the splitting of the pressure into inertial and polymeric contributions, it is shown that the trains of cylindrical structures around sheets of high polymer extension that are characteristics to elasto-inertial turbulence are mostly driven by polymeric contributions.

INTRODUCTION

Polymer additives are known for producing upward of 80% drag reduction in turbulent wall-bounded flows through strong alteration and reduction of turbulent activity (White & Mungal, 2008). The changes in flow dynamics induced by polymers do not lead to flow relaminarization but, at most, to a universal asymptotic state called maximum drag reduction (MDR, Virk *et al.* 1970). At the same time, polymer additives have also been shown to promote transition to turbulence (Hoyt, 1977), or even lead to a chaotic flow at very low Reynolds number as in elastic turbulence (Groisman & Steinberg, 2000).

These seemingly contradicting effects of polymer additives can be explained by the interaction between elastic instabilities and the flow's inertia characterizing elasto-inertial turbulence, hereafter referred to as EIT (Samanta *et al.*, 2012; Dubief *et al.*, 2013). EIT is a state of small-scale turbulence that exists by either creating its own extensional flow patterns or by exploiting extensional flow topologies. EIT provides answers to phenomena that current understanding of MDR cannot, such as the absence of log-law in finite-Reynolds numbers MDR flows (White *et al.*, 2012), and the phenomenon of early turbulence. Moreover, it supports De Gennes (1990)'s picture that drag reduction derives from two-way energy transfers between turbulent kinetic energy of the flow and elastic energy of polymers at small scales, resulting in an overall modification of the turbulence energy cascade at high Reynolds numbers.

As shown by the viscoelastic pipe experiment of Samanta *et al.* (2012), an elastic instability can occur at a Reynolds number smaller than the transition in Newtonian pipe flow if the polymer concentration and Weissenberg number are sufficiently large. Moreover, it was observed that the measured friction factor then follows the characteristic MDR friction law. These findings were also confirmed by direct numerical simulations as shown in Figure 1 (Dubief *et al.*, 2013). The analysis of these simulations showed that thin sheets of locally high polymer stretch, tilted upwards and elongated in the flow direction, create trains of spanwise cylindrical structures of alternating sign, as shown in Figure 2. This feature of EIT disappears when the flow is too turbulent or the polymer solution not elastic enough, which led to the hypothesis that EIT is an asymptotic state that should occur when the elasticity of the solution can efficiently control and contain the growth of turbulence.

Dubief *et al.* (2013) suggested that the formation of sheets of polymer stretch results from the unstable nature of the nonlinear advection of low-diffusivity polymers. These sheets, hosting a significant increase in extensional viscosity, create a strong local anisotropy, with a formation of local low-speed jet-like flow. The response of the flow is through pressure, whose role is to redistribute energy across components of momentum, resulting in the formation of waves, or trains of alternating rotational and straining motions. Once triggered, EIT is self-sustained since the elas-

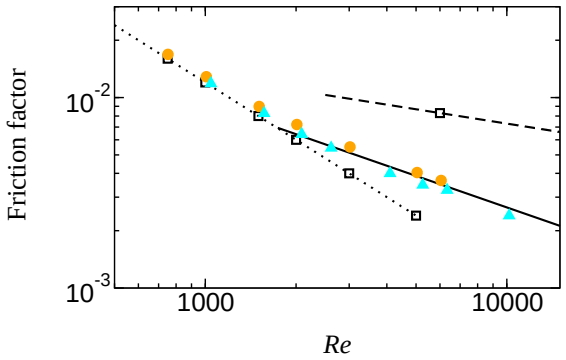

Figure 1. Friction factor as a function of the Reynolds number for two Weissenberg numbers $Wi = 100$ (●), $Wi = 700$ (▲). Lines indicate correlations for laminar (⋯⋯ , $f = 12/Re$) and turbulent (– – – – , $f = 0.073Re^{-1/4}$) Newtonian channel flow and for MDR (——— , $f = 0.42Re^{-0.55}$); Newtonian solutions are also included (□).

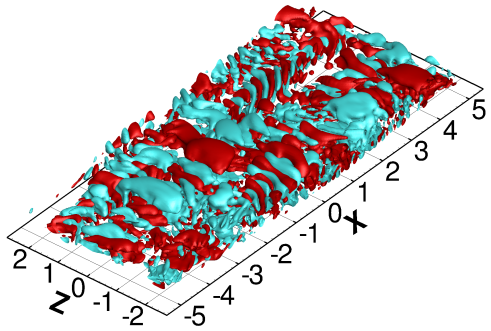

Figure 2. Instantaneous isosurface of the second invariant Q_a of the velocity gradient tensor in the lower half of the channel for $Re = 1000$ and $Wi = 8$; $Q_a = 0.025$ (red) and $Q_a = -0.025$ (cyan).

tic instability creates the very velocity fluctuations it feeds upon.

The underlying mechanism driving EIT is here further investigated through an analysis of the pressure, and its interaction with topological structures of the flow and polymer stress. The approach relies on the splitting of the pressure into inertial and polymeric contributions following the methodology of Mansour *et al.* (1988) and Kim (1989).

METHOD

Direct numerical simulations

Channel flow simulations are performed in a cartesian domain, where x, y and z are the streamwise, wall-normal and spanwise directions, respectively. For a polymer solution, the flow transport equations are the conservation of mass, $\nabla \cdot \mathbf{u} = 0$, where $\mathbf{u} = (u, v, w)$ is the velocity vector, and transport of momentum:

$$\partial_t \mathbf{u} + (\mathbf{u}\cdot\nabla)\mathbf{u} = -\nabla p + \frac{\beta}{Re}\nabla^2\mathbf{u} + \frac{1-\beta}{Re}\nabla\cdot\mathbf{T}\,. \quad (1)$$

The Reynolds number is based on the bulk velocity U_b and the full channel height $H = 2h$, $Re = U_b H/\nu$. The polymer stress tensor $\mathbf{T}$ is computed using the FENE-P model:

$$\mathbf{T} = \frac{1}{Wi}\left(\frac{\mathbf{C}}{1-\mathrm{tr}(\mathbf{C})/L^2} - \mathbf{I}\right)\,, \quad (2)$$

where $\mathbf{I}$ is the unit tensor and $\mathbf{C}$ the polymer conformation tensor, whose transport equation is

$$\partial_t \mathbf{C} + (\mathbf{u}\cdot\nabla)\mathbf{C} = \mathbf{C}(\nabla\mathbf{u}) + (\nabla\mathbf{u})^{\mathrm{T}}\mathbf{C} - \mathbf{T}\,. \quad (3)$$

The properties of the polymer solution are the ratio β of solvent viscosity to the zero-shear viscosity of the solution, the maximum polymer extension L, and the Weissenberg number $Wi = \lambda\dot{\gamma}$ based on the solution relaxation time λ and the wall shear-rate $\dot{\gamma}$ of the initial laminar flow at each Re. Eqs. (1-3) are solved using finite differences on a staggered grid and a semi-implicit time advancement scheme (Dubief *et al.*, 2005). A thorough resolution study led us to choose a domain size of $10H \times H \times 5H$ with $256 \times 151 \times 256$ computational nodes. All results have been verified on domains with a factor 2 in horizontal dimensions and resolution in each directions. The CFL number was set to 0.15 to guarantee the boundedness of $\mathbf{C}$.

Three different cases are considered here: $Re = 1000$ at $Wi = 8$ ($Wi^+ = 24$), and $Re = 6000$ at $Wi = 8$ ($Wi^+ = 96$) and $Wi = 60$ ($Wi^+ = 720$). The lower Reynolds number corresponds to a subcritical flow ($Re < Re_c$, where $Re_c = 1791$ defines the intersection between the laminar and MDR friction drag lines as shown in Figure 1), while the larger Reynolds number corresponds to a value for which the Newtonian flow is turbulent. The Weissenberg numbers at $Re = 6000$ are chosen to achieve high drag reduction (HDR) and MDR, respectively. For all three cases $L = 200$ and $\beta = 0.9$ were used. The corresponding statistics can be found in Dubief *et al.* (2013).

Inertial and polymeric contributions to pressure

In order to investigate the role of pressure in the mechanism underlying EIT, a similar approach to Mansour *et al.* (1988) and Kim (1989) is followed. Taking the divergence of the momentum equation (1) leads to a Poisson equation for the pressure:

$$\nabla^2 p = 2Q_a + \frac{1-\beta}{Re}\nabla\cdot(\nabla\cdot\mathbf{T})\,, \quad (4)$$

where $Q_a = -1/2\partial_i u_j \partial_j u_i = -1/2\partial_i\partial_j(u_i u_j)$ is the second invariant of the velocity gradient tensor. In contrast to a Newtonian flow, a second term appears on the right-hand side, which represents the contribution from the polymeric stress. For a periodic channel flow, the pressure satisfies equation (4) with the boundary condition

$$\left.\frac{\partial p}{\partial y}\right|_{y=\pm h} = \left.\frac{\beta}{Re}\frac{\partial^2 v}{\partial y^2}\right|_{y=\pm h} + \left.\frac{1-\beta}{Re}\frac{\partial^2 T_{yy}}{\partial y^2}\right|_{y=\pm h} \quad (5)$$

at the walls and periodicity in x and z.

By splitting the right-hand side of Eq. 4 into different terms and separating the effect of the wall boundary condition, their respective contributions to the total pressure can

be isolated. In particular, we consider here following splitting for the pressure fluctuations $p'(\mathbf{x}) = p(\mathbf{x}) - \overline{P}(\mathbf{x})$:

$$p'(\mathbf{x}) = p'_r(\mathbf{x}) + p'_s(\mathbf{x}) + p'_p(\mathbf{x}) + p'_{St}(\mathbf{x}) \,, \tag{6}$$

where fluctuations are denoted by $\cdot'$ and mean quantities by $\bar{\cdot}$. The first three contributions on the right-hand side of Eq. (6) are solutions of (Gerolymos *et al.*, 2013):

$$\nabla^2 p'_r = -2\frac{\mathrm{d}\overline{U}}{\mathrm{d}y}\frac{\partial v'}{\partial x} \,, \tag{7}$$

$$\nabla^2 p'_s = -\frac{\partial u'_i}{\partial x_j}\frac{\partial u'_j}{\partial x_i} + \frac{\mathrm{d}^2\overline{v'^2}}{\mathrm{d}y^2} \,, \tag{8}$$

$$\nabla^2 p'_p = \frac{1-\beta}{\mathrm{Re}}\frac{\partial^2 T'_{ij}}{\partial x_i \partial x_j} \,, \tag{9}$$

with the homogeneous wall boundary condition

$$\left.\frac{\partial p'_r}{\partial y}\right|_{y=\pm h} = \left.\frac{\partial p'_s}{\partial y}\right|_{y=\pm h} = \left.\frac{\partial p'_p}{\partial y}\right|_{y=\pm h} = 0 \,. \tag{10}$$

The 'rapid' part, p'_r, is linear in the velocity fluctuations and represents the immediate response to a change imposed on the mean field, while the 'slow' part, p'_s, feels this change through nonlinear interactions (Kim, 1989). In addition to these two inertial terms, the pressure in a viscoelastic flow also has an elastic contribution, p'_p, originating in the polymeric stress. Finally, the effect of the wall boundary condition is represented by the Stokes pressure, p'_{St}, which satisfies

$$\nabla^2 p'_{St} = 0 \tag{11}$$

with the inhomogeneous boundary condition

$$\left.\frac{\partial p'_{St}}{\partial y}\right|_{y=\pm h} = \left.\frac{\beta}{Re}\frac{\partial^2 v'}{\partial y^2}\right|_{y=\pm h} + \left.\frac{1-\beta}{Re}\frac{\partial^2 T'_{yy}}{\partial y^2}\right|_{y=\pm h} \,. \tag{12}$$

As the Stokes pressure is typically much smaller than the other contributions, it is not considered here.

This pressure split is applied to the simulation results for the three cases mentioned above and statistics are computed in order to identify the relative contributions from inertia and elasticity, as shown below.

RESULTS

Equations (7)-(9) have been solved with homogeneous wall boundary condition to obtain the three contributions p'_r, p'_s and p'_p. About 500 fields have been collected for each of the three cases considered, on which statistics have been performed.

Statistics

The root-mean-square (r.m.s.) values of the different pressure contributions and of their sum across the channel

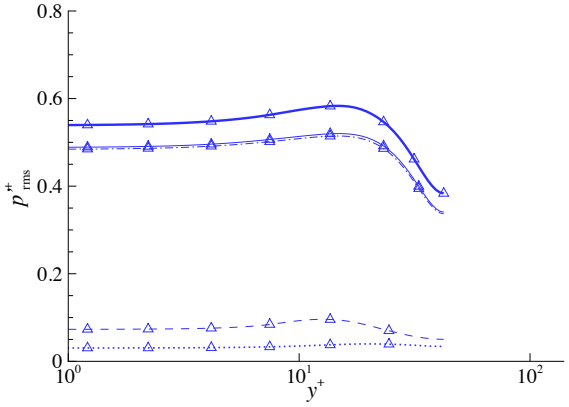

Figure 3. R.m.s. of the different pressure contributions as a function of y^+ for $Re = 1000$, $Wi = 8$. p'_r: —·—; p'_s: ·····; p'_p: – – – –; $p'_{rs} = p'_r + p'_s$: ———; $p'_{rsp} = p'_r + p'_s + p'_p$: ▬▬.

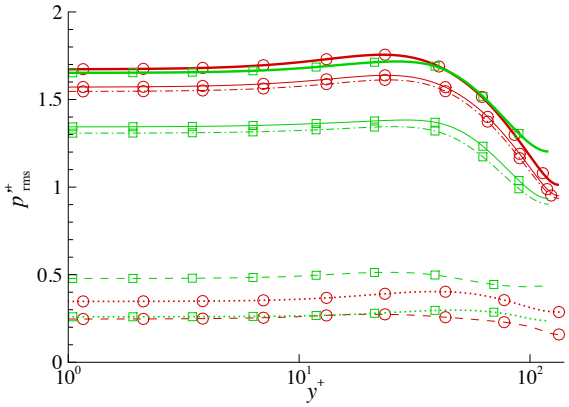

Figure 4. R.m.s. of the different pressure contributions as a function of y^+ for $Re = 6000$, $Wi = 8$ (HDR, ○) and $Re = 6000$, $Wi = 60$ (MDR, □). Line style same as Figure 3.

height are shown in Figures 3 and 4[1]. It can be observed that the dominating contribution comes from the rapid pressure. In contrast to a Newtonian turbulent channel flow, where the slow part dominates (Gerolymos *et al.*, 2013), the slow pressure is here much lower, illustrating the drag-reduced state of the flow at $Re = 6000$; it is even almost negligible at $Re = 1000$. Moreover, both rapid and slow parts are slightly larger for the second case (HDR) than for the third case (MDR), as it could be expected. On the other hand, the elastic pressure, absent in the Newtonian case, has a non-negligible contribution in all cases. Figure 5 shows the ratio of the r.m.s. of the elastic pressure p'_p to the inertial pressure, $p'_{rs} = p'_r + p'_s$, indicating that the polymer contribution is about 15% of p'_{rs} at $Wi = 8$ and increases to about 35-40% at the larger Weissenberg number. Generally, the polymer pressure is larger than the slow part, except in the HDR case ($Re = 6000$, $Wi = 60$). Finally, note that the splitting into an inertial and elastic contribution is a simplified view as the polymer stress in Eq. (1) can create velocity fluctuations and, thus, indirectly contributes to the inertial pressure and conversely, as it will be discussed below.

Dubief *et al.* (2013) suggested that the role of pressure is to redistribute turbulent kinetic energy across components of momentum, resulting in the formation of waves, or trains

[1] Note that $\overline{p'^2_{rsp}} = \overline{(p'_r + p'_s + p'_p)^2} \neq \overline{p'^2_r} + \overline{p'^2_s} + \overline{p'^2_p}$.

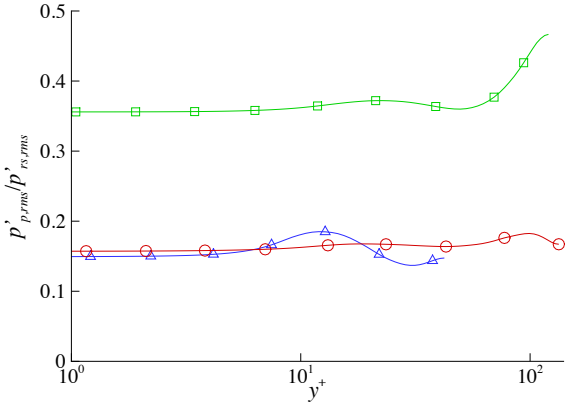

Figure 5. Ratio of the polymeric to the inertial pressure r.m.s. as a function of y^+. $Re = 1000$, $Wi = 8$: △; $Re = 6000$, $Wi = 8$: ○; $Re = 6000$, $Wi = 60$: □.

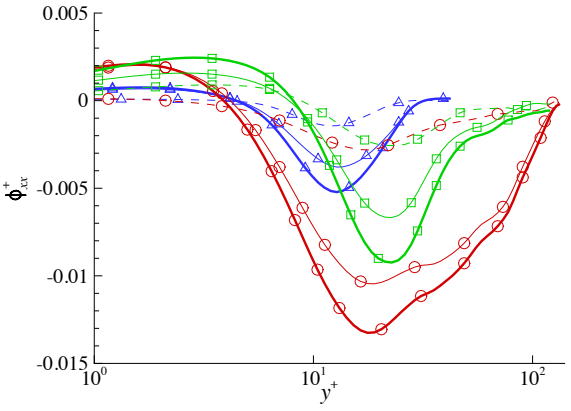

Figure 6. Contributions to the pressure-strain component ϕ^+_{xx} as a function of y^+. $Re = 1000$, $Wi = 8$: △; $Re = 6000$, $Wi = 8$: ○; $Re = 6000$, $Wi = 60$: □. p'_p: – – – – ; $p'_{rs} = p'_r + p'_s$: ——— ; $p'_{rsp} = p'_r + p'_s + p'_p$: ▬▬ .

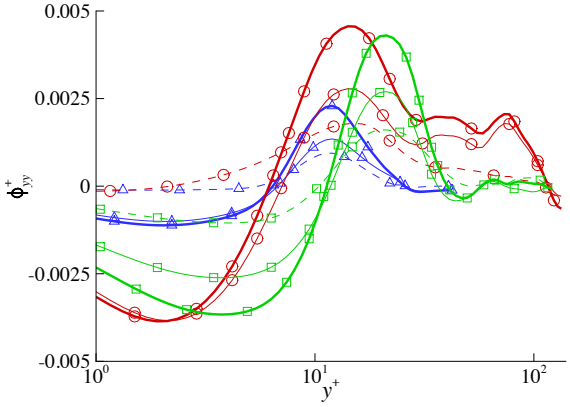

Figure 7. Contributions to the pressure-strain component ϕ^+_{yy} as a function of y^+. Same line style and symbols as Figure 6.

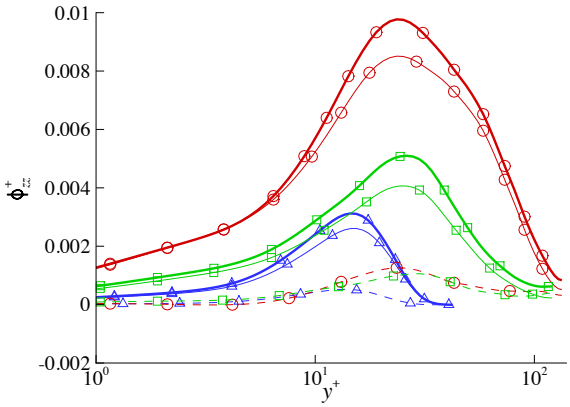

Figure 8. Contributions to the pressure-strain component ϕ^+_{zz} as a function of y^+. Same line style and symbols as Figure 6.

of alternating rotational and straining motions. To illustrate this, the terms containing pressure in the Reynolds stress transport equations are further analyzed. The velocity-pressure gradient correlation

$$\Pi_{ij} = -\overline{u'_i \frac{\partial p'}{\partial x_j}} - \overline{u'_j \frac{\partial p'}{\partial x_i}} \tag{13}$$

can be separated into two contributions, $\Pi_{ij} = \phi_{ij} + d^{(p)}_{ij}$, representing the pressure-strain and the pressure-diffusion, respectively (Gerolymos *et al.*, 2013). They are defined as

$$\phi_{ij} = \overline{p' \left(\frac{\partial u'_i}{\partial x_j} + \frac{\partial u'_j}{\partial x_i} \right)}, \tag{14}$$

$$d^{(p)}_{ij} = \overline{\frac{\partial p' u'_i}{\partial x_j} + \frac{\partial p' u'_j}{\partial x_i}}. \tag{15}$$

The contributions to the pressure-strain components ϕ_{xx}, ϕ_{yy} and ϕ_{zz} are shown in Figures 6-8. Their qualitative behavior is very similar to a Newtonian flow at a similar Reynolds number (Gerolymos *et al.*, 2013), but with lower levels owing to the turbulence reduction. Additionally, the contributions from p'_p and p'_{rs} are qualitatively similar, with a lower level for the polymeric part. However, the polymeric contribution is comparatively larger for ϕ_{yy}, while lower for ϕ_{zz}, which would tend to indicate that the elastic contribution slightly favors a two-dimensional flow, the three-dimensionality being mostly driven by the inertial part. As the pressure-strain tensor is by definition deviatoric, it does not make any contribution to the turbulent kinetic energy, but rather redistributes energy between its different components. In all cases, a clear transfer of turbulent kinetic energy from the streamwise component (negative ϕ_{xx}) to both the wall-normal and spanwise components (positive ϕ_{yy} and ϕ_{zz}) can be observed for $y^+ \gtrsim 10$, highlighting the role of pressure in redistributing the energy. Note however that ϕ_{xx} is negative and ϕ_{yy} positive very close to the wall. Similar conclusions can be drawn from Π_{ij} and $d^{(p)}_{ij}$ (not shown here). Finally, unlike Newtonian flows, the larger contribution to the pressure-strain comes from the rapid part, except for the HDR case, where both rapid and slow contributions are of similar magnitude. This seems to indicate that MDR flows are characterized by a dominating contribution of the rapid pressure, or more exactly by a stronger attenuation of the slow part.

A major qualitative difference from a Newtonian turbulent flow is observed for the $x-y$ component. In particular, Π_{xy} (see Figure 9) is negative (i.e., production of Reynolds stress) around $y^+ \approx 10$. This behavior is directly caused by the polymer pressure and could partly explain the small but non-vanishing Reynolds stress seen in such flows.

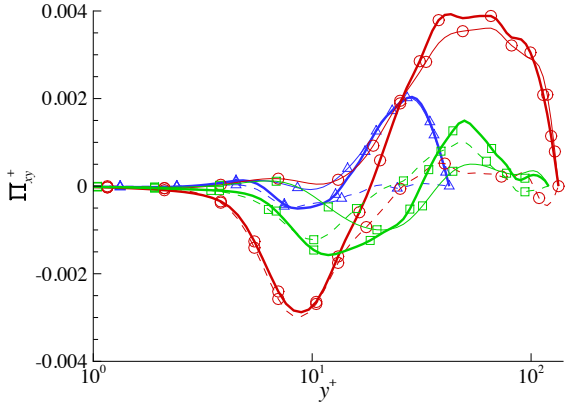

Figure 9. Contributions to the velocity-pressure gradient correlation component Π^+_{xy} as a function of y^+. Same line style and symbols as Figure 6.

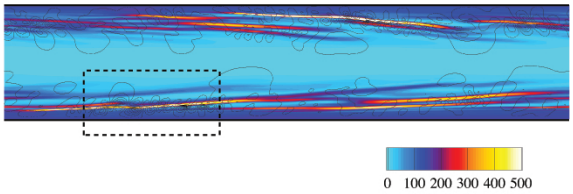

Figure 10. Instantaneous contour of the polymer stress component T_{xx} and isolines of Q_a (dash lines represent negative values) in a $x-y$ plane for $Re = 1000$ and $Wi = 8$. The flow is from left to right and the dashed box represents the region plotted in the next two figures.

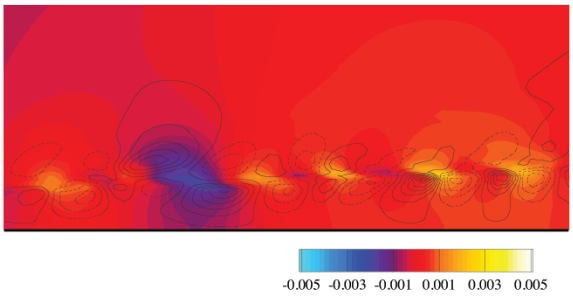

Figure 11. Instantaneous contour of the pressure contribution p_p and isolines of Q_a (dash lines represent negative values) in a $x-y$ plane for $Re = 1000$ and $Wi = 8$. The region plotted corresponds to the dashed box in Figure 10.

Instantaneous fields

As shown in Figure 2, the flow is characterized by trains of cylindrical Q_a structures of alternating sign around thin sheets of large polymer extension. This is further illustrated in Figure 10, which shows the contour of the polymer stress component T_{xx} and isolines of Q_a in a $x-y$ plane for the lower Reynolds number case. The long thin sheets of large polymer extension and cylindrical structures are clearly visible.

A small region of the $x-y$ plane around one of these sheets is shown in Figures 11 and 12. The first figure illustrates the link between the polymer pressure p_p and the Q_a structures. The largest fluctuations of p_p are of alternating sign and located on each side of the sheet, mostly between the cylindrical Q_a structures. The wavelength of these structures is the same as the wavelength of the Q_a structures. On the other hand, the inertial pressure, p_{rs} does not show such a clear correlation. Large fluctuations of p_{rs} are rather correlated with the center of strong Q_a structures, as shown in Figure 12. In particular, as in inertial turbulence, positive values of Q_a correspond to low pressure regions, and thus, to vortical regions (Dubief & Delcayre, 2000). The analysis of the polymer body force $\mathbf{f}_p = \nabla \cdot \mathbf{T}$ (not shown here) indicates that the polymer body force is mostly parallel to the sheet with opposite sign on each side. Additionally, $\mathbf{f}_p$ also alternates direction along the sheet with the same wavelength as the Q_a structures and opposite sign, indicating that the polymers are most likely the driving force that creates these structures.

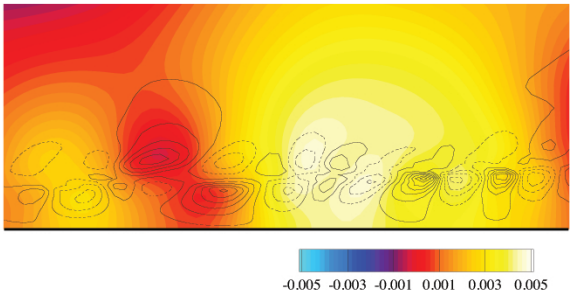

Figure 12. Instantaneous contour of the pressure contribution p_{rs} and isolines of Q_a (dash lines represent negative values) in a $x-y$ plane for $Re = 1000$ and $Wi = 8$. The region plotted corresponds to the dashed box in Figure 10.

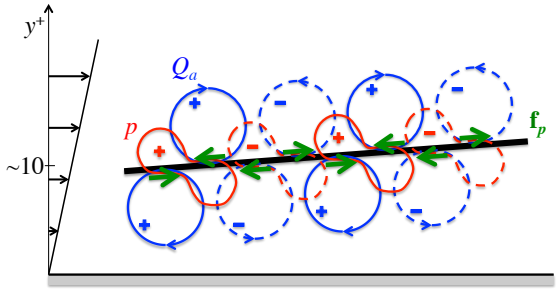

Figure 13. Schematics of the typical structures observed around thin sheets of large polymer extension (black line) in the near-wall region: second invariant of the velocity gradient tensor Q_a (blue), pressure p (red) and polymer body force $\mathbf{f}_p = \nabla \cdot \mathbf{T}$ (green). Dotted lines indicate a negative value.

The overall picture gained from this analysis is schematically summarized in Figure 13. The combined effect of advection at low diffusivity and existing flow perturbations leads to the formation of sheets of high polymer extension and, in turn, to a large increase in the extensional viscosity, and thus in the polymer stress. Small perturbations of the sheets cause the polymer body force to alternate direction, and thereby, create these cylindrical Q_a structures. The pressure adapts to ensure zero divergence of the velocity and redistribute part of the turbulent kinetic energy from the streamwise to the other components. Once triggered, this process appears to be self-sustained, at least over the hundreds of flow through-time simulated here. Therefore, it can be conjectured that these characteristic trains of cylindrical structures are mostly driven by the polymers. Nonetheless, an indirect effect from inertia most probably

also contributes to the dynamics. Further analysis is still required to ascertain this.

CONCLUSION AND FUTURE WORK

An analysis of the role of pressure in the dynamics of EIT has been presented. The splitting of the pressure into different components, in particular into an elastic and an inertial part, has provided a tool to assess the relative contributions of both components to the overall dynamics. It was shown that the elastic, or polymer, pressure is a non-negligible component of the total pressure fluctuations, although the rapid part dominates. Unlike Newtonian flows, the slow part is much lower in elasto-inertial turbulence. Statistics have also demonstrated the redistributive role of pressure. Finally, a schematic description of the typical structures encountered in EIT was proposed. It is postulated that those small-scales structures, associated with thin sheets of large polymer extension, are directly driven by the polymers. Nonetheless, an indirect inertial contribution is still possible, and most likely required for a self-sustaining dynamics.

In a broader context, elasto-inertial turbulence offers a new perspective on polymer drag reduction. First it provides support to De Gennes (1990)'s theory of energy transfers between polymers and flow. Second, EIT allows to consider the possible structure of MDR for very large elasticity ($Wi \to \infty$): the sheer magnitude of extensional viscosity is likely to prevent the emergence of any vortical structures, thus leaving MDR to be sustained by near-wall spanwise structures similar to the ones observed at low-Reynolds numbers (Figure 2 and 11). As discussed by Dubief *et al.* (2012), the flow is therefore stuck in a transitional state, specifically the stage of breakdown of nonlinear flow instabilities, which does not support a logarithmic mean velocity profile (Klewicki *et al.*, 2011).

Many questions remain unanswered, such as the mechanism by which small perturbations of the sheet lead to a body force of alternating sign, the role of those elastic instabilities and the validity of the above conclusions at larger Reynolds number, the possible existence of these instabilities in two-dimensions, ... Further analysis is thus required to obtain a definite description of the physical mechanisms underlying EIT, which will be part of future work.

ACKNOWLEDGMENTS

The Vermont Advanced Computing Center is gratefully acknowledged for providing the computing resources. YD acknowledges the support of grant No. P01HL46703 (project 1) from the National Institutes of Health. VET acknowledges the financial support of a Marie Curie FP7 Career Integration Grant (Grant No. PCIG10-GA-2011-304073). JS acknowledges the support of the Australian Research Council. This work was initiated during the Center for Turbulence Research 2012 Summer Program.

REFERENCES

De Gennes, P.G. 1990 *Introduction to Polymer Dynamics*. Cambridge University Press.

Dubief, Y. & Delcayre, F. 2000 On coherent-vortex identification in turbulence. *J. of Turbulence* **1** (011).

Dubief, Y., Terrapon, V.E. & Soria, J. 2013 On the mechanism of elasto-inertial turbulence. `http://arxiv.org/abs/1301.3952` Submitted to Phys. Fluids.

Dubief, Y., Terrapon, V.E., White, C.M., Shaqfeh, E.S.G., Moin, P. & Lele, S.K. 2005 New answers on the interaction between polymers and vortices in turbulent flows. *Flow, Turbulence and Combustion* **74** (4), 311–329.

Dubief, Y., White, C.M., Shaqfeh, E.S.G. & Terrapon, V.E. 2012 Polymer maximum drag reduction: A unique transitional state. *Phys. Fluids* Submitted.

Gerolymos, G.A., Sénéchal, D. & Vallet, I. 2013 Wall effects on pressure fluctuations in turbulent channel flow. *J. Fluid Mech.* **720**, 15–65.

Groisman, A. & Steinberg, V. 2000 Elastic turbulence in a polymer solution flow. *Nature* **405** (6782), 53–55.

Hoyt, J.W. 1977 Laminar-turbulent transition in polymer solutions. *Nature* **270**, 508–509.

Kim, J. 1989 On the structure of pressure fluctuations in simulated turbulent channel flow. *J. Fluid Mech.* **205**, 421–451.

Klewicki, J., Ebner, R. & Wu, X. 2011 Mean dynamics of transitional boundary-layer flow. *J. Fluid Mech.* **682**, 617–651.

Mansour, N.N., Kim, J. & Moin, P. 1988 Reynolds-stress and dissipation-rate budgets in a turbulent channel flow. *J. Fluid Mech.* **194** (1), 15–44.

Samanta, D., Dubief, Y., Holzner, M., Schäfer, C., Morozov, A., Wagner, C. & Hof, B. 2012 Elasto-inertial turbulence. `http://arxiv.org/abs/1212.6392` Submitted to PNAS.

Virk, P.S., Mickley, H.S. & Smith, K.A. 1970 The ultimate asymptote and mean flow structure in Toms phenomenon. *Trans. ASME E: J. Appl. Mech* **37**, 488–493.

White, C.M., Dubief, Y. & Klewicki, J. 2012 Re-examining the logarithmic dependence of the mean velocity distribution in polymer drag reduced wall-bounded flow. *Phys. Fluids* **24** (2), 021701–021701.

White, C.M. & Mungal, M.G. 2008 Mechanics and prediction of turbulent drag reduction with polymer additives. *Annu. Rev. Fluid Mech.* **40** (1), 235–256.